A study of the electromagnetic proton cyclotron instability as a generation mechanism for EMIC waves in the Earth's magnetosphere using SCATHA data

Son T. Nguyen,[1] J. D. Perez,[2] and Joseph F. Fennell[3]

Received 22 January 2007; revised 6 July 2007; accepted 11 September 2007; published 4 December 2007.

[1] Using 59 days of magnetic field data from SCATHA, a study of the electromagnetic proton cyclotron instability as a generation mechanism for EMIC waves in the Earth's magnetosphere has been conducted. From 1181 events found, we selected 373 events that were not influenced by the presence of He^+ and O^+ ions, i.e., events with frequency above the local He^+ cyclotron frequency and that had all the required accompanying data. These events occurred in all magnetic local times (MLT) sectors, with L ranging from 5.6 to 8.1 and magnetic latitudes (MLAT) from $-13.7°$ to 15.6°. Assuming a pure proton plasma, the proton temperature anisotropy, A_p, is determined from the maximum normalized frequency at which power is emitted. Using measured parameters and estimated total number density, the convective growth rate, S, of Electromagnetic Ion Cyclotron (EMIC) waves as a function of frequency depends only on the parallel proton temperature, $T_{\|}$. Matching the observed peak in the frequency spectrum and the calculated peak in S allows the determination of $T_{\|}$ and the proton perpendicular temperature, $T_{\perp}$, for each event. Analysis of the results yields a new empirical expression for A_p as a function of the hot proton parallel beta, $\beta_{\|h}$, and the maximum value of the wave temporal growth rate. The relationship between A_p and $\beta_{\|h}$ is consistent with theoretical predictions. The dependence of A_p on $T_{\|}$ is consistent with the expectation that the free energy source of EMIC waves is energetic protons with $T_{\perp} > T_{\|}$.

Citation: Nguyen, S. T., J. D. Perez, and J. F. Fennell (2007), A study of the electromagnetic proton cyclotron instability as a generation mechanism for EMIC waves in the Earth's magnetosphere using SCATHA data, *J. Geophys. Res.*, *112*, A12203, doi:10.1029/2007JA012291.

1. Introduction

[2] Electromagnetic Ion Cyclotron (EMIC) waves, with frequencies from ~0.1 to 5.0 Hz, have been observed in the equatorial region of the magnetosphere by numerous geostationary and elliptically orbiting spacecraft, such as ATS-1, ATS-6, DE-1, ISEE-1/2, AMPTE/CCE, and CRRES. EMIC waves have been observed on the ground as geomagnetic pulsations. They are expected to be generated most favorably in the equatorial region and amplified at the expense of energetic (ten to several hundred keV) protons with an anisotropic ($T_{\perp} > T_{\|}$) population through an electromagnetic ion cyclotron instability [e.g., *Cornwall*, 1965; *Kennel and Petschek*, 1966; *Gary et al.*, 1994a].

[3] The studies of *Bossen et al.* [1976] (ATS-1), *Kaye and Kivelson* [1979] (OGO-5), *Fraser* [1985] (ATS-6), *Ishida et al.* [1987] (ATS-6), and *Anderson et al.* [1990] (AMPTE/CCE) showed that EMIC waves occurred in the equatorial region over a wide range of L values from L ~ 3 to the region near the magnetopause. *Anderson et al.* [1992a], using data from the AMPTE/CCE satellite which covered the region from L = 3.5 to 9 at magnetic latitudes (MLAT) between $-16°$ and 16°, found that EMIC waves were more common at high L (L > 7) than at low L (L < 6) and occurred mainly from 03:00 to 09:00 magnetic local times (MLT) and from 10:00 to 18:00 MLT. A study by *Fraser and Nguyen* [2001], using data from the CRRES satellite which covered the radial region of L = 3.5–8 and MLAT between $-30°$ and 30°, showed that EMIC waves occurred both inside and outside the plasmapause in the afternoon sector with a clear peak around 14:00 to 16:00 MLT and also in the morning sector with a minor peak around 05:00 to 07:00 MLT. The MLT distribution of EMIC wave occurrence in the equatorial region of the magnetosphere is consistent in the two studies of *Anderson et al.* [1992a, Figure 8] and *Fraser and Nguyen* [2001, Figure 6].

[4] Since the discovery of heavy ions such as He^+, O^+ in the magnetospheric plasma, many studies have shown that these ions have profound effects on EMIC wave propagation and generation [e.g., *Young et al.*, 1981; *Perraut et al.*, 1984; *Fraser et al.*, 1992; *Kozyra et al.* [1997]; *Thorne and*

[1]The Pre-University School of Hochiminh City, Hochiminh City, Vietnam.
[2]Allison Laboratory, Auburn University, Auburn, Alabama, USA.
[3]Space Science Laboratory, the Aerospace Corporation, El Segundo, California, USA.

0148-0227/07/2007JA012291

Horne, 1997; *Jordanova et al.*, 2001]. The presence of these ions introduces additional resonance, cut-off, crossover frequencies, and multiion hybrid frequencies and polarization reversals in the wave propagation process.

[5] The effects of He^+ ions on the wave propagation and generation were studied by *Young et al.* [1981], *Roux et al.* [1982], *Rauch and Roux* [1982], *Perraut et al.* [1984], and *Fraser et al.* [2005]. It may be expected that the presence of O^+ ions has similar effects on the wave propagation and generation. Observations of the effects of O^+ ions are hampered, however, by the fact that the characteristic frequencies introduced by the presence of O^+ ions are in the 0.1–0.2 Hz band and close to spacecraft spin frequencies [e.g., *Fraser et al*., 1992].

[6] *Fraser and McPherron* [1982], using ATS-6 satellite data, found that the spectra of the observed waves revealed slots near the equatorial helium and oxygen cyclotron frequencies (see Figure 10 in their paper). According to their results, 78 EMIC waves were observed over the four-month interval. Nineteen of them revealed slots associated with the presence of O^+ ions, thirty associated with the presence of He^+ ions, and three with the presence of both He^+ and O^+ ions.

[7] The calculations of the wave convective growth rate in a multicomponent plasma including H^+, He^+, and O^+ ions by *Gomberoff and Cuperman* [1982], *Gomberoff and Neira* [1983], and *Kozyra et al.* [1984] showed that the presence of He^+ and O^+ ions introduces corresponding spectral slots or stop bands in the wave power spectrum. Besides H^+ ions, *Gomberoff and Cuperman* [1982] considered only cold He^+ ions and showed that the presence of these ions introduces a stop band at $X \sim 0.25$ (the local Helium gyrofrequency F_{CHe}), where X is the ratio of the observed frequency to the local proton gyrofrequency. *Gomberoff and Neira* [1983] considered only cold O^+ and He^+ ions and show that their presence introduces stop bands at $X \sim 0.0625$ (the local Oxygen gyrofrequency F_{CO}) and at $X \sim 0.25$, respectively. *Kozyra et al.* [1984] considered both cold and hot He^+ and O^+ ions and showed that in general the presence of these ions introduces stop bands at F_{CO} and F_{CHe}. Moreover, their results showed that energetic He^+ and O^+ ions not only produce ion cyclotron wave growth rates at frequencies below the corresponding gyrofrequencies (F_{CHe} and F_{CO}) but also suppress partially or completely the wave growth rates at frequencies above the corresponding gyrofrequencies (for example, see their Figure 15). *Fraser et al.* [1989] used the formula established by *Kozyra et al.* [1984] to calculate convective growth rates of EMIC waves, assuming a H^+-He^+-O^+ plasma with relative densities of 8–10% He^+ and less than 1% O^+, to explain the EMIC waves observed by ISEE 1 at $L = 4.9 \pm 0.1$. The results showed an agreement between the wave packet bounce periods, measured from the observed dynamic spectra, and those calculated independently for parallel propagation.

[8] In a theoretical study, *Kozyra et al*. [1997] modeled the contribution of EMIC waves to stormtime ring current erosion, using a multicomponent plasma with H^+, He^+, and O^+ ions. They found that a region of strong EMIC wave activity forms just inside and along the plasmapause and the loss timescale of H^+ ions due to wave scatterings is ~11 h. Similarly, *Jordanova et al.* [2001] also modeled ring current proton precipitation by EMIC waves and used a multicomponent plasma with relative densities of ~4% He^+ and 30% O^+, respectively. Their results showed that the most intense fluxes of precipitating protons are observed along the duskside plasmapause during the main and early recovery phases of the storm and are caused by scatterings of EMIC waves, consistent with *Kozyra et al*. [1997].

[9] *Thorne and Horne* [1997] showed that during moderate magnetic storms, the presence of O^+ ions with a peak of energy at $L \leq 3$ and high relative densities of up to 30% (compared to a typical value of 10% and a energy peak at $L = 5$ during geomagnetically quiet periods) can have a strong controlling effect on the excitation of EMIC waves. For the most intense magnetic storms, the presence of O^+ ions with relative densities greater than 60% can suppress the wave excitation in the band above F_{CO}. *Thorne and Horne* [1994] showed that the growth rate of EMIC waves in the band above F_{CO} can also be partially suppressed by the presence of cyclotron resonant energetic O^+ ions, consistent with the results of *Kozyra et al.* [1984].

[10] Recently, *Fraser et al.* [2005], using data from GOES-8, GEOS-10, LANL, and IMAGE, showed that EMIC waves may be preferentially generated in enhanced plasma density created by the plasma plume. A slot in the wave spectrum was observed, suggesting the presence of He^+ ions with relative densities in the range from 6% to 16%, in a predominantly H^+ plasma.

[11] In the studies by *Gomberoff and Cuperman* [1982], *Gomberoff and Neira* [1983], *Kozyra et al.* [1984], and *Fraser et al.* [1989], the energetic (hot) ion population distributions are assumed to be bi-Maxwellian for the calculations of wave convective growth rates. This is consistent with the proton population observed by ATS-6, which was used to investigate the electromagnetic proton cyclotron instability by *Mauk and McPherron* [1980, Figure 7]. The study by *Anderson et al.* [1996] using AMPTE/CCE data, however, found that the anisotropy of the observed hot proton distributions was energy-dependent and that in the energy range from 1 to 50 keV these distribution are not well characterized by a bi-Maxwellian distribution (see Figures 1 and 2 in their paper). On the other hand, bi-Maxwellian proton distributions with $T_\perp > T_\parallel$ have been commonly observed in the magnetosphere [e.g., *Anderson and Hamilton*, 1993; *Kallenrode*, 2001]. Specifically, *Anderson and Hamilton* [1993, Figures 6–8] showed 16-min average proton distributions observed by AMPTE/CCE that were bi-Maxwellian.

[12] Theoretical and experimental studies on the electromagnetic proton cyclotron instability have been carried out by many authors [e.g., *Gary et al.*, 1994a; *Gary and Lee*, 1994; *Anderson et al.*, 1994, 1996; *Samsonov et al.*, 2001, A. A. Samsonov et. al, Proton temperature anisotropy in the magnetosheath: comparison of 3-D MHD modelling with Cluster data, submitted to *Ann. Geophys.*, 2006, hereinafter referred to as A. A. Samsonov et. al, submitted manuscript, 2006]. These studies showed that there is an inverse correlation between proton temperature anisotropy A_p, defined as

$$A_p = \frac{T_\perp}{T_\parallel} - 1 \tag{1}$$

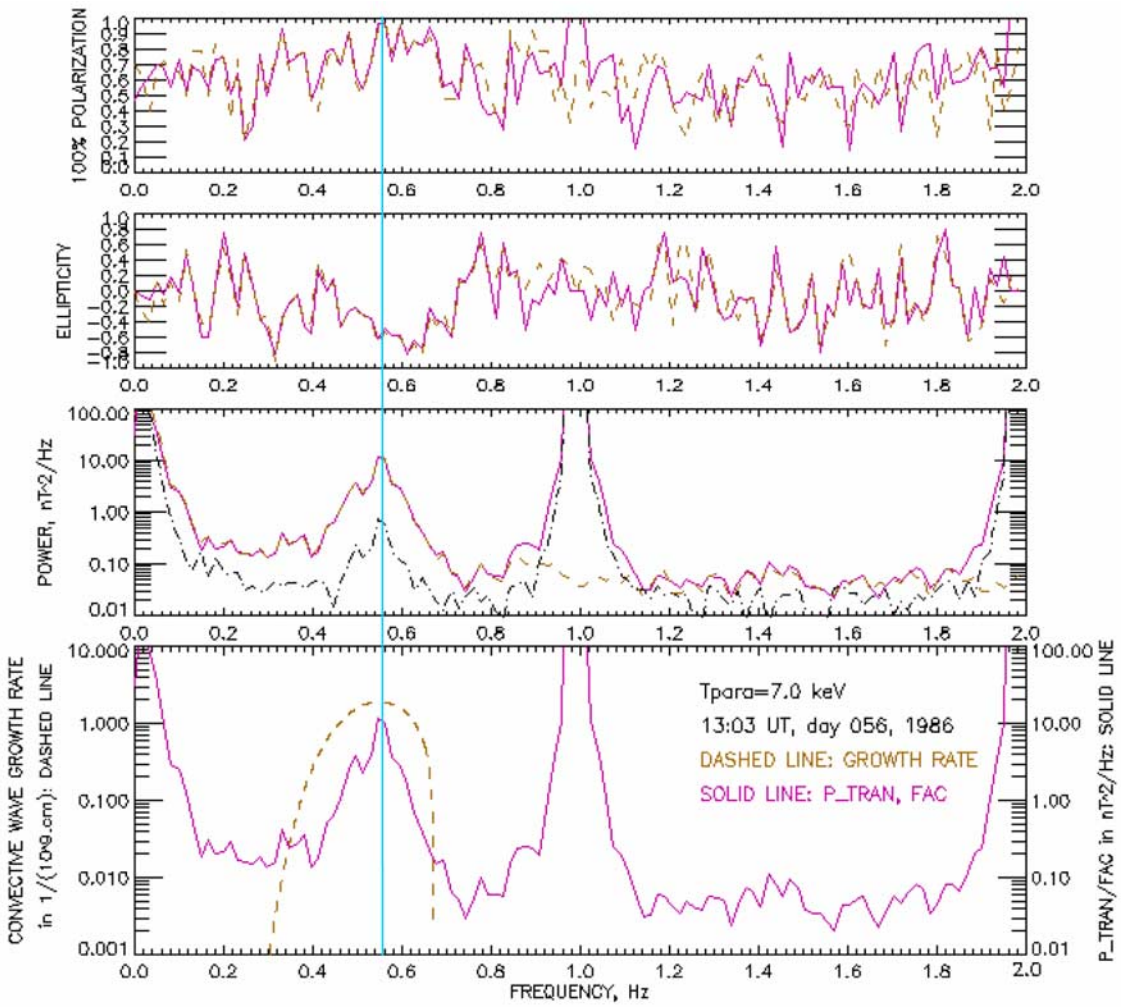

Figure 1. From top to bottom, the first panel shows the plots of wave percent polarization versus frequency in the FAC (solid pink line) and GSM (dashed brown line) coordinate systems for the 2-minute interval beginning at 13:03 UT, day 056; the second shows those of ellipticity. The third shows the wave spectra for the same event; the solid pink line is P_{tran} in FAC; the dot-dashed black line is P_{para} in FAC; and the dashed brown line is P_{tran} in GSM. The fourth shows the plots of the calculated convective growth rate S (dashed brown line) and P_{tran} in FAC (solid pink line) versus frequency for the same event.

and hot proton parallel beta $\beta_{\|h}$ for this instability. $\beta_{\|h}$ is defined as follows

$$\beta_{\|h} = \frac{2\mu_o n_h k_B T_\|}{B_o^2} \quad (2)$$

where n_h is the hot proton number density and B_o the ambient magnetic field strength.

[13] Several experimental studies of the electromagnetic proton cyclotron instability in the magnetosphere have been conducted [e.g., *Mauk and McPherron*, 1980; *Anderson et al.*, 1996]. *Mauk and McPherron* [1980] used data from the ATS-6 geostationary satellite to show a good match between predicted and measured frequencies, which is strong evidence that the linear, proton cyclotron instability mechanism is responsible for the observed EMIC waves. The study by *Anderson et al.* [1996], using data from the AMPTE/CCE satellite, showed that the occurrence of EMIC waves in the magnetosphere is consistent with the predictions of the linear instability theory of electromagnetic proton cyclotron waves, demonstrating the predictive capability of this theory. *Anderson et al.* [1996], however, covered only dawn and noon wave events with L > 7. In the current study, by using data from the SCATHA satellite we extend the range of observations to all local time sectors with L values from 5.6 to 8.1 and MLAT from $-13.7°$ to $15.6°$.

[14] This paper is organized as follows. Section 2 is devoted to instrumentation, data preparation, and event selection. Section 3 describes the methodology of this study and gives details of the analysis implementation. Section 4 gives an example. Section 5 discusses the results. Section 6 presents the conclusions drawn from this study.

2. Data Description and Preparation

2.1. Instrumentation

[15] The data we use in this study are from the experiments on board the SCATHA (P78-2) spacecraft. SCATHA stands for Spacecraft Charging At High Altitude. The

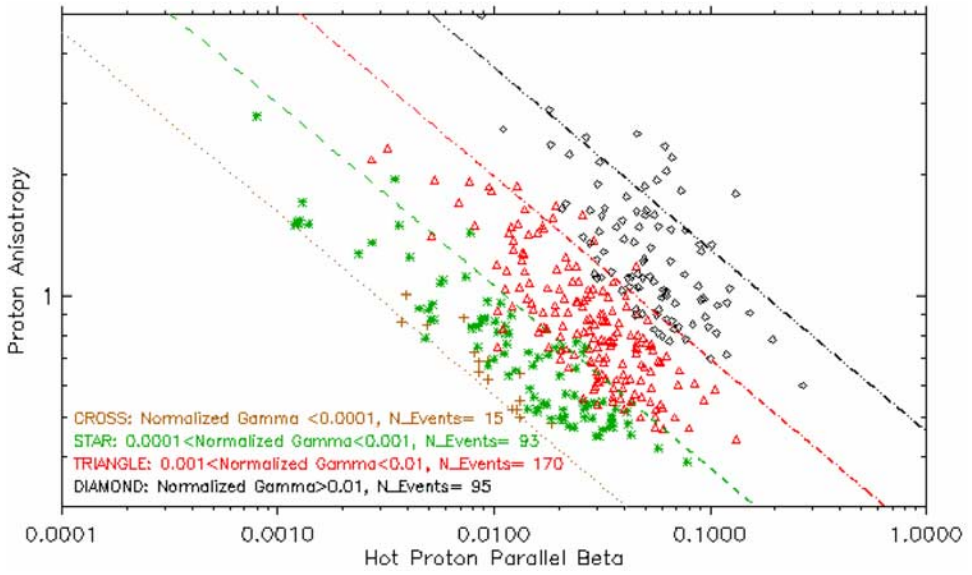

Figure 2. A scatterplot of proton temperature anisotropy A_p versus hot proton parallel beta $\beta_{\|h}$ with the data binned by maximum normalized temporal growth rate values, γ_m/Ω_p, and color-coded. The dotted brown line depicts the $A_p - \beta_{\|h}$ relation with $\gamma_m/\Omega_p = 10^{-4}$; the long-dashed green line with $\gamma_m/\Omega_p = 10^{-3}$; the dot-dashed red line for $\gamma_m/\Omega_p = 10^{-2}$, and the dot-dot-dashed black line for $\gamma_m/\Omega_p = 10^{-1}$.

spacecraft was launched in January 1979 into a near-synchronous orbit with a perigee of 5.3 R_E, apogee of 7.8 R_E, and an inclination to the equatorial plane of 7.8°. The primary mission of SCATHA was to obtain information on the processes and effects of spacecraft charging. Its specific objectives included (1) obtaining environmental and engineering data to allow the creation of design criteria, materials, techniques, tests, and analytical methods to control charging of spacecraft surfaces and (2) collecting scientific data about plasma wave interactions, substorms, and the energetic ring current. More details on the satellite, descriptions of the experiments on board, its scientific objectives, measuring techniques, and operational aspects can be found in the paper by *Stevens and Vampola* [1978].

[16] The satellite's orbital period was ~23.6 h, resulting in an eastward drift in longitude at a rate of ~5.3° per day and a good radial coverage at all MLTs. The spacecraft was spin stabilized with a spin period of one minute, and the spin axis was in the orbital plane and maintained approximately perpendicular to the Sun-Earth line.

[17] The satellite's mission lasted nearly 12 full years and returned comprehensive particle and field measurements of the near-equatorial and near-synchronous space environment [*Spence et al.*, 1997]. Through a recovery effort at the Aerospace Corporation, these data have recently been made available. According to *Fennell et al.* [1997], the recovery effort produced High Resolution (HR) and Summary data sets which consist of data from the experiments: (a) SC1-8 experiment for measurements of VLF magnetic and electric wavefields, (b) SC2 experiment for measurements of suprathermal plasma and energetic protons, (c) SC3 experiment for measurements of high energy electrons, (d) SC10 experiment for measurements of electric field, and (f) SC11 experiment for measurements of magnetic field.

[18] The HR data sets consist of the highest time resolution measurements from these experiments. These measurements have been converted to physical units and written onto magneto-optical disks in CDF format [*Fennell et al.*, 1997]. The HR data sets have been further processed to get Summary data at ~1-min intervals. In this study we employed 59 days (year 1986) of HR magnetic field measurements from the SC11 experiment. We also used average energetic (0.15 keV to 133 keV) proton number density, n_h, and spacecraft ephemeris data, i.e., magnetic local times (MLT), magnetic latitudes (MLAT), L shell values, and spacecraft geocentric radii (ERAD). These data were included in the Recovery Summary data. Further details are provided by *Fennell et al.* [1997].

2.2. Data Preparation and Event Selection

[19] The three-component magnetic data sampled at 4 Hz, obtained by the SCATHA satellite, were first detrended using polynomial curve fitting, and data gaps and spikes were removed. A transformation from the GSM coordinate system to a field-aligned coordinate (FAC) system was then carried out. A Hamming window was applied to the time series, and the mean was removed prior to fast Fourier transformation (FFT) and spectral analysis.

[20] The FFT length is chosen to be N = 240, resulting in a frequency resolution of 0.017 Hz ($\Delta f = 1/(2N\Delta t)$, Δt = 0.25 sec). Wave spectra were obtained for transverse ($[\delta B_x^2 + \delta B_y^2]^{1/2}$) and parallel components with respect to the local ambient magnetic field $\mathbf{B_o}$ over the frequency range from 0 to 2 Hz. The Nyquist frequency is 2 Hz ($f_{Nyq} = 1/(2\Delta t)$).

[21] We calculated from the data the wave ellipticity ε, defined as the ratio of the minor to major axis of the polarization ellipse, and the degree of polarization (or percent polarization), defined as the ratio of coherent power to total power. Wave power spectral density, ellipticity, and degree of polarization values are extracted at 2-min intervals with 0.25-s resolution to give quantitative measures of the power spectral density (PSD) transverse to $\mathbf{B_o}$, P_{tran}, and

power spectral density parallel to $\mathbf{B_o}$, P_{para}. These values were generated for both field-aligned coordinate (FAC) system and GSM coordinate system. In the GSM coordinate system, we consider B_z as the 'parallel' component, and the 'transverse component' means the component perpendicular to B_z. In fact, in the equatorial region of interest in this study, the local z direction in the GSM coordinate system usually makes a small angle with respect to that of the local magnetic field line in the L range considered here.

[22] The P_{tran} spectra obtained in the FAC system show spin effects at 1 Hz and 2 Hz, but the P_{tran} spectra obtained in the GSM coordinate system do not. For any particular 2-min interval, we found that, in the neighborhood of the peak, the dependence of P_{tran} on frequency in both coordinate systems is almost the same, and the magnitudes of P_{tran} in the two coordinate systems are different from one another by a nearly constant factor, whose value depends on the 2-min interval considered. Therefore for frequency and ellipticity in the neighborhood of the peak we use P_{tran} in the GSM coordinate system in place of P_{tran} in the FAC system without losing any information.

[23] To allow quantitative analysis of a rather large quantity of data, each power spectrum of 480 points, corresponding to 2 min of data, was scanned automatically for peaks in the wave spectrum. To identify EMIC wave candidates, the following criteria were used: (1) The peak spectral power of transverse component P_{tran} must be at least one order of magnitude greater than the corresponding power background. (2) The peak frequency is above the Pc 3 range, i.e., $\geq$0.1 Hz. The Nyquist frequency in this study is 2 Hz so the range of peak frequency is from 0.1 to 2 Hz. This covers the range of Pc 2 waves (0.1–0.2 Hz) and part of the range of Pc 1 waves (0.2–5 Hz). This choice of frequency range is expected to capture the majority of EMIC wave events, as data from 700 CRRES orbits showed that less than 5% of the total number of EMIC wave events observed had frequencies above 2 Hz and no EMIC waves with frequencies above 4 Hz were found [e.g., *Fraser and Nguyen*, 2001]. (3) In the neighborhood of the peak, the magnitude of P_{tran} must be significantly greater than that of P_{para} in the FAC system. Visual inspection of spectra, i.e., the corresponding plots of P_{tran} and P_{para} versus frequency in both coordinate systems for each 2-min interval, was also performed to make sure only true EMIC waves were identified. In the 59 days of data examined, there were 1181 wave events defined as a 2-min interval during which EMIC waves occur with at least one peak in the transverse power as a function of frequency.

[24] In order to focus upon events that were not influenced by the presence of He^+ and O^+ ions, we considered events with frequency above the local He^+ cyclotron frequency. We then included only events for which SCATHA data provided the hot proton number density n_h needed for the calculation of the wave convective growth rate *S*. This resulted in the analysis of 373 events.

3. Methodology

3.1. Electromagnetic Proton Cyclotron Instability

[25] Standard theories of waves in magnetized plasmas [e.g., *Swanson*, 2003] show that EMIC waves are generated when the proton perpendicular temperature, $T_\perp$, is greater than the proton parallel temperature, $T_\parallel$. As pointed out by *Gary et al.* [1976], when $T_\perp > T_\parallel$, the electromagnetic proton cyclotron instability is not the only instability that may arise. However, for a pure proton plasma, the electromagnetic proton cyclotron instability with $\mathbf{k} \times \mathbf{B_o} = 0$, i.e., parallel propagation, and with left-hand circular polarization is the mode with the fastest growth rate [*Gary*, 1993]. Therefore we will use the results from theoretical treatments of EMIC waves in the magnetosphere to analyze the events found from the SCATHA data.

3.2. Estimation of Proton Temperature Anisotropy

[26] For each selected event we obtain the frequencies f_{peak}, f_{Max}, and f_{Min}. Where the peak frequency f_{peak} corresponds to the maximum value of P_{tran}; f_{Max} and f_{Min} are the frequencies on either side of the peak frequency at which P_{tran} reduces to the power background. We always have $f_{Min} < f_{peak} < f_{Max}$ for any event. The experiments on board SCATHA also give us the local magnetic field strength B_o from which we calculate frequency normalized to the local proton gyrofrequency denoted as *X*. The hot proton density n_h is also given in the Summary data. Using the available values of MLT, MLAT, L, and ERAD (distance from the Earth's center to the location of interest), we estimate the value of the local total electron number density, *n*, from the empirical models of *Chappell* [1974], *Sheeley et al.* [2001], and *Denton et al.* [2002]. Thus from the SCATHA data, we obtain the parameters needed for the calculations of linear convective growth rates of EMIC waves.

[27] As pointed out by *Kozyra et al.* [1984], the effective amplification of waves in the Earth's magnetosphere depends on the time spent by the waves traveling through the growth region, which is of finite extent. Thus the relevant quantity is the wave convective growth rate *S* rather than the temporal growth rate γ. *S* is the ratio of γ and the wave group velocity v_g.

[28] In this study to calculate S, we use the formula established by *Gomberoff and Neira* [1983] for parallel propagation of EMIC waves in a pure proton plasma with the assumption that the distribution of energetic proton population is bi-Maxwellian. Because we only consider events with frequencies higher than the local He+ gyrofrequency, we omit contributions from all ions except protons so the formula is

$$S = \frac{\gamma}{v_g} = \frac{\sqrt{\pi}}{2\alpha_\parallel}\left[A_p(1-X) - X\right] \cdot \exp\left\{\frac{-(1-X)^2}{\beta_{\parallel h} X^2}\left(\frac{1+\delta}{1-X}\right)\right\} \Big/ \left[X^2\left(\frac{1+\delta}{1-X}\right)\right] \quad (3)$$

where k_B is the Boltzmann constant, $\delta = n_{pc}/n_h$ the relative (cold to hot) proton number density, n_{pc} the cold proton number density, $\alpha_\parallel = (2k_B T_\parallel/m_p)^{1/2}$ the proton parallel thermal velocity, and m_p the mass of proton.

[29] As pointed out in the introduction, the assumption of a bi-Maxwellian distribution for the protons is not always valid [e.g., *Anderson et al.*, 1996]. *Xue et al.* [1996] studied the growth rate of EMIC waves in the magnetosphere using an anisotropic kappa (generalized Lorentzian), instead of bi-Maxwellian, particle distribution to model the energetic

ring current ions. Their calculations for kappa distributions under magnetospheric conditions of moderately disturbed activities and a nominal relative Helium concentration of 10%, showed that the results obtained with a bi-Maxwellian distribution tended to overestimate the peak convective growth rate for EMIC waves but did not show a strong influence on the peak frequency [see their Figure 3, Figures 5 and 6 (lower panel)]. Therefore we expect the determination of A_p, $T_{\|}$, and $T_{\perp}$ to be insensitive to the assumption of a bi-Maxwellian distribution function for the protons.

[30] For EMIC waves, $0 < \omega < \Omega_p$, where $\omega = 2\pi f$ and $\Omega_p = 2\pi F_{CH} = qB_o/m_p$, thus we are interested in $0 < X < 1$, and, from equation (3), we see that if other parameters are kept constant, the sign of S depends upon the difference

$$\Delta = A_p - \frac{X}{1-X} \tag{4}$$

First we see that we only get growth ($S > 0$) when $X < 1$. We also see that growth stops ($S = 0$) when $\Delta = 0$, so we identify the corresponding normalized frequency as X_{Max}, the frequency at which the EMIC emissions end, i.e.,

$$A_p - \frac{X_{Max}}{1-X_{Max}} = 0 \tag{5}$$

As a result, we can determine A_p from the observed X_{Max}.

3.3. Estimation of Proton Parallel Temperature

[31] With the availability of MLT, MLAT, L, and ERAD values, the local total electron number density n was estimated by using the empirical models. The proton number density n_h was also included in the SCATHA Summary data, as noted in section 2.1. Having obtained n and n_h, we deduce the cold proton number density n_{pc} by using the charge quasi-neutrality condition.

[32] From equation (3) we can see that given B_o, n, n_h, and A_p, the value of wave convective growth rate S as a function of X or frequency f has the proton parallel temperature $T_{\|}$ as the only remaining undetermined parameter. Assuming that the peak frequency in the observed emission spectrum corresponds to the calculated peak in the convective growth rate allows the determination of $T_{\|}$. With A_p and $T_{\|}$ available, the proton perpendicular temperature $T_{\perp}$ is also obtained from equation (1).

[33] For examining polarization properties of the observed waves, for each event we also calculated ε_{peak} and ε_{ave}, where ε_{peak} is the value of ellipticity at the peak frequency, and ε_{ave} is the ellipticity weighted by transverse spectral power, i.e., $\varepsilon_{ave} = \sum_{f_{Min}}^{f_{Max}} \varepsilon P_{tran} \,/\, \sum_{f_{Min}}^{f_{Max}} P_{tran}$, averaged over the frequency range from f_{Min} to f_{Max}.

[34] For each event, we determined the value of $T_{\|}$ with a resolution of 0.1 keV that gave the same calculated and observed peak frequency. $T_{\perp}$ was calculated by using equation (1), and $\beta_{\|h}$ was also calculated by using equation (2). For a comparison of the frequency spread of the calculated S about the peak frequency with that of the observed P_{tran}, we also calculated the 'minimum' frequency of S, f_{Min_S}, at which the corresponding calculated value of the convective wave growth rate, S_{Min}, satisfies $S_{Min}/S_{peak} = P_{tran\_Min}/P_{tran\_peak}$, where P_{tran_Min} and P_{tran_peak} are the values of P_{tran} in the GSM coordinate system at $f = f_{Min}$ and $f = f_{peak}$, respectively, and $S_{peak} = S_{Max}$ the value of S at f_{peak}, i.e., the maximum value of S. We found that the difference between the observed f_{Min} and the calculated f_{Min_S} was significant for only 2% of 373 events considered. The matching of the observed and the calculated features of the EMIC emission spectra supports the validity of the methodology and procedures employed in this study.

4. Example

[35] We now consider in detail a typical 2-min EMIC wave event, centered at 13:03 UT and occurring at 12.00 MLT, L = 7.2, 6.9° MLAT, on day 056, 1986. From top to bottom, the first panel of Figure 1 shows the plots of the wave percent polarization versus frequency in the FAC (the solid pink line) and GSM (the dashed brown line) coordinate systems for this event; the second shows the wave ellipticity. The third shows the wave spectra for the same event; the solid pink line is P_{tran} in the FAC system; the dot-dashed black line is P_{para} also in the FAC system; and the dashed brown line is P_{tran} in the GSM coordinate system. The fourth panel shows the plots of the calculated wave convective growth rate S (the dashed brown line) and P_{tran} in the FAC system (the solid pink line) versus frequency for the same event.

[36] From the first and second panels, we see (follow the vertical blue line from the top) that in the neighborhood of the peak frequency, the values of percent polarization and ellipticity in the FAC (the solid pink lines) and GSM (the dashed brown lines) coordinate systems are almost equal. From the third panel, we also see that in the neighborhood of the peak frequency, the dependences of P_{tran} on frequency in the two coordinate systems are nearly the same (the solid pink line and the dashed brown line), and the magnitudes of P_{tran} in the two system are different from one another by a nearly constant factor. From this panel, the spin effects in the FAC system at 1 Hz and 2 Hz are clearly seen in P_{tran} (the solid pink line) and P_{para} (the dot-dashed black line), but no spin effects are seen in P_{tran} (the dashed brown line) in the GSM coordinate system. Thus we use P_{tran} in the GSM coordinate system multiplied by the appropriate factor in place of P_{tran} in the FAC system. Also from the third panel, we see that in the neighborhood of the peak frequency, the value of P_{tran} (the solid pink line) is approximately an order of magnitude greater than that of P_{para} (the dot-dashed black line) in the FAC system, confirming the field-aligned propagation of the EMIC waves in this event.

[37] For this event we found that $f_{peak} = 0.55$ Hz, $f_{Max} = 0.67$ Hz, $f_{Min} = 0.42$ Hz, the local magnetic field strength $B_o = 106$ nT, the measured proton hot density $n_h = 0.12$ cm^{-3} (from the SCATHA Summary data), and the total electron number density is taken to be n = 5.2 cm^{-3} from the models. The peak ellipticity and averaged ellipticity for this event are $\varepsilon_{peak} = -0.68$ and $\varepsilon_{ave} = -0.52$, respectively, thus the observed waves are typically left-hand polarized.

[38] Following the procedures outlined in sections 2.2 and 3, we obtained $A_p = 0.7$, $T_{\|} = 7.0$ keV, $T_{\perp} = 11.9$ keV, and $\beta_{\|h} = 0.03$. We found $f_{Min\_S} = 0.41$ Hz, and the difference between f_{Min} and f_{Min_S} is only 0.01 Hz. The calculated convective growth rate as a function of frequency for this event (the dashed brown line in the fourth panel) is

Table 1a. Summary of the Relationship Between A_p and $\beta_{\|h}$ Through the Coefficients S_h and α_h of the Relation $A_p = S_h(\gamma_m/\Omega_P)^M \beta_{\|h}^{\alpha_h}$ and the Correlation Coefficients R for Different MLT Sectors

MLT	S_h	α_h	M	Range of γ_m/Ω_p	R	No. of Events
03 < MLT < 09 (Dawn sector)	0.62	−0.49	0.23	$2 \times 10^{-5} - 4 \times 10^{-2}$	−0.97	67
09 < MLT < 15 (Noon sector)	0.84	−0.51	0.30	$4 \times 10^{-5} - 1 \times 10^{-1}$	−0.97	256
15 < MLT < 21 (Evening sector)	0.82	−0.39	0.24	$1 \times 10^{-4} - 2 \times 10^{-2}$	−0.98	22
21 < MLT < 03 (Midnight sector)	0.43	−0.42	0.15	$5 \times 10^{-5} - 7 \times 10^{-3}$	−0.87	28
All	0.86	−0.45	0.27	$2 \times 10^{-5} - 1 \times 10^{-1}$	−0.89	373

compared to P_{tran} in the FAC system (the solid pink line in the same panel) for $T_{\|} = 7.0$ keV in the neighborhood of the peak frequency. We see the agreement among the minimum, peak, and maximum frequencies, but the observed frequency spectrum is narrower than the calculated one. This could be due to approximations such as assuming a bi-Maxwellian for the proton distribution function in this analysis.

5. Results and Discussions

[39] The 373 events are binned by MLT, ε_{ave}, and L values. The result of binning by MLT values shows that 67 events occurred between 03 and 09 MLT, the dawn sector; 256 between 09 and 15 MLT, the noon sector; 22 between 15 and 21 MLT, the evening sector; and 28 from 21 MLT through midnight to 03 MLT, the midnight sector. The number of events occurring in the noon sector is greater than those in the other local time sectors, in agreement with the result of *Anderson et al.* [1992a] using AMPTE/CCE data which cover nearly the same MLAT range as ours, as shown in their Figure 8. The result of binning by ε_{ave} values shows that 208 events occurred with ε_{ave} between −1 and −0.1, treated as left-hand polarized; 100 with ε_{ave} between −0.1 and 0.1, linearly polarized; and 65 with ε_{ave} between 0.1 and 1, right-hand polarized. This result is consistent with that of *Anderson et al.* [1992b] (see the bottom panel of Figure 6 in their paper) and that of *Fraser and Nguyen* [2001] (see Figure 10 in their paper). Binning the data by L values shows that 20 events occurred in the region of L between 5.6 and 6; 90 in that of L between 6 and 7; and 263 with L between 7 and 8.1. The number of events occurring in the region of L between 7 and 8.1 is greater than that in the region between 5.6 and 7, consistent with the finding of *Anderson et al.* [1992a] that EMIC waves were more common at high L (L > 7) than at low L (L < 6), as mentioned in section 1.

5.1. Inverse Correlation Between Proton Temperature Anisotropy and Proton Parallel Beta

[40] In a simulation study, *Gary et al.* [1994a] showed that, in the framework of the linear instability theory, the threshold value of the proton temperature anisotropy is related to the hot proton parallel beta by the expression

$$A_p = S_p \beta_{\|h}^{\alpha} \tag{6}$$

where S_p is of order unity, but varies as a function of temporal growth rate, and $\alpha \cong -0.40$ ($\alpha < 0$) independent of temporal growth rate for $0.05 \leq \beta_{\|h} \leq 5.0$. Experimentally, *Anderson and Fuselier* [1993] and *Anderson et al.* [1994] using the AMPTE/CCE satellite data for the subsolar magnetosheath region found the same functional form of the relation between A_p and $\beta_{\|h}$ as equation (6) with $S_p = 0.85$ and $\alpha = -0.48$, showing that the observed anisotropy values were close to the thresholds. In the dawn sector of the magnetosphere, *Anderson et al.* [1996] studied EMIC waves with L > 7 using data from the AMPTE/CCE satellite and found that the values of A_p were also near the threshold values as expected. They found the same empirical relationship applied in this region as in the magnetosheath for active times with S_p the same and only a slight change in α from −0.48 to −0.52. In the noon sector of the magnetosphere, however, the *Anderson et al.* [1996] data showed $S_p = 0.2$, much smaller than that in the dawn sector. They attributed the lower limit for the noon events to the presence of unmeasured cold plasma. *Kennel and Petschek* [1966] pointed out that a sufficient anisotropy is required for EMIC waves to grow and wave particle interactions will then force the particle distribution toward a marginal linear stability state. The anisotropy causing the wave growth is therefore diminished and subsequent wave growths slowed, leading to a final state where the plasma remains close to the ion cyclotron instability threshold curve.

[41] In the current study we use the following equation

$$A_p = S_h(\gamma_m/\Omega_P)^M \beta_{\|h}^{\alpha_h} \tag{7}$$

where $\gamma_m = S_{Max} v_g$ is the calculated maximum value of wave temporal growth rate, and S_h, M, and α_h are constants. It is to be noted that the assumption of bi-Maxwellian distributions for the proton distribution function may have some impact here. As stated above, *Xue et al.* [1996] found that distributions that show a strong departure from bi-Maxwellian often give lower growth rates. This would produce a different scaling in equation (7), but would not be expected to change the features of the results.

[42] By comparing (6) and (7), we see that S_p in (6) corresponds to the product $S_h (\gamma_m/\Omega_P)^M$ in (7). It means that we now have the explicit dependence of S_p on the wave temporal growth rate and there is also an inverse relation between A_p and $\beta_{\|h}$. We found corresponding values of S_h, M, and α_h by fitting data from all the events and also from different MLT sectors and L ranges. A fit to our full data yields $S_h = 0.87$, $M = 0.27$, and $\alpha_h = -0.45$ with a correlation coefficient $R = -0.89$. A fit to the data for each local time sector results in different values of S_h, M, α_h, and R, as shown in Table 1a. From the table, for the dawn sector with L > 7, we have $S_h = 0.62$ and $\alpha_h = -0.49$; these values are different from those of *Anderson et al.* [1996] ($S_p = 0.85$ and $\alpha = -0.52$); this difference may be due to the fact

Table 1b. Summary of the Relationship Between A_p and $\beta_{\|h}$ Through the Coefficients S_h and α_h of the Relation $A_p = S_h(\gamma_m/\Omega_P)^M \beta_{\|h}^{\alpha_h}$ and the Correlation Coefficients R for Different L Ranges

L value	S_h	α_h	M	Range of γ_m/Ω_p	R	No. of Events
L < 6	0.78	−0.27	0.15	$1 \times 10^{-4} - 2 \times 10^{-2}$	−0.97	20
6 < L < 7	0.54	−0.39	0.19	$4 \times 10^{-5} - 1 \times 10^{-2}$	−0.90	90
L > 7	0.83	−0.50	0.29	$2 \times 10^{-5} - 1 \times 10^{-1}$	−0.91	263
All	0.86	−0.45	0.27	$2 \times 10^{-5} - 1 \times 10^{-1}$	−0.89	373

that we used more events (67) than they did (12) and they considered events with the averaged value of maximum normalized temporal growth rate, γ_m/Ω_p, of 2.5×10^{-2}, much greater than the value of 0.5×10^{-2} for the 67 events considered here. Higher γ_m/Ω_p correspond to more energy that the waves can get from the interacting proton populations and thus higher A_p are expected. From the table, we also see that the observed inverse correlation is good with R ranging from −0.87 to −0.97 and the value of α_h is nearly stable.

[43] A fit to the data for each radial region results in different values of S_h, M, α_h, and R, as shown in Table 1b. From the table, we also see that the observed inverse correlation is good with R ranging from −0.89 to −0.97 and the value of α_h is also nearly stable.

[44] The finding that S_h varies with MLT sector and L range is in agreement with the argument by *Gary et al.* [1994b] that this coefficient depends on macroscopic factors, particularly how hard external forces drive the energetic proton temperature anisotropy.

[45] *Gary et al.* [1994a] used the linear Vlasov theory, with the value of $T_{\|e}/T_{\|p} = 0.25$, where $T_{\|e}$ is the electron parallel temperature, and the normalized Alfven velocity of $v_A/c = 10^{-4}$, and found that in equation (6) $S_p = 0.35$ and $\alpha = -0.42$ for $\gamma_m/\Omega_p = 10^{-4}$; $S_p = 0.43$ and $\alpha = -0.42$ for $\gamma_m/\Omega_p = 10^{-3}$; $S_p = 0.65$ and $\alpha = -0.40$ for $\gamma_m/\Omega_p = 10^{-2}$. *Samsonov et al.* [2001] solved the linear Vlasov dispersion equation as a function of $\beta_{\|h}$ for a pure proton plasma to find the threshold conditions for the electromagnetic cyclotron instability and the mirror instability assuming fixed γ_m/Ω_p for each instability, and found that equation (6) holds for both instabilities. For the electromagnetic cyclotron instability, their results gave the values of S_p and α that are almost equal to those found by *Gary et al.* [1994a], for $0.01 \leq \beta_{\|h} \leq 10.0$ and the same three values of γ_m/Ω_p, see Figure 1 in their paper. Recently, A. A. Samsonov et. al, submitted manuscript, 2006, using magnetosheath data from Cluster, found that for low $\beta_{\|h}$ ($\beta_{\|h} < 1.0$) the observed proton temperature anisotropy A_p is in agreement with the proton cyclotron threshold and for higher $\beta_{\|h}$ ($\beta_{\|h} \geq 1.0$) the observed A_p is close to both proton cyclotron threshold and mirror threshold, as shown in their Figure 10. To compare our results with those of *Gary et al.* [1994a], we produced a scatterplot of A_p versus $\beta_{\|h}$ with data binned by values of γ_m/Ω_p and color-coded, as shown in Figure 2. In this figure, the dotted brown line depicts the observed $A_p - \beta_{\|h}$ relation with $\gamma_m/\Omega_p = 10^{-4}$, of the form $A_p = 0.39\beta_{\|h}^{-0.39}$; the long-dashed green line with $\gamma_m/\Omega_p = 10^{-3}$, of the form $A_p = 0.65\beta_{\|h}^{-0.39}$; the dot-dashed red line for $\gamma_m/\Omega_p = 10^{-2}$, of the form $A_p = 1.10\beta_{\|h}^{-0.39}$; and the dot-dot-dashed black line for $\gamma_m/\Omega_p = 10^{-1}$, of the form $A_p = 1.84\beta_{\|h}^{-0.39}$. From Figure 2, we also see that the A_p value in the different ranges are near the corresponding threshold lines, in agreement with the findings of *Kennel and Petschek* [1966], as mentioned earlier in this section.

5.2. Dependence of Proton Temperature Anisotropy on Proton Parallel Temperature

[46] The upper panel of Figure 3 shows a scatterplot of A_p versus $T_\|$ with the data binned by MLT values and color-coded; the dotted line is the fitting curve for all data. The lower panel shows those binned by L values. From either panel, we see that for EMIC waves to be destabilized in general lower $T_\|$ requires higher A_p. This is consistent with a finding that the free energy source of EMIC waves is energetic protons with an anisotropic distribution. Consider two energetic and anisotropic ($T_\perp > T_\|$) proton populations with the same $T_\|$, and we expect that the one with higher A_p can give more energy to the waves than the other. As a result, given a low value of $T_\|$ the corresponding value of $T_\perp$ must be high enough so that A_p is high enough to give sufficient energy for the waves to grow or to be amplified. From each panel, we also see that A_p and $T_\|$ approximately follow the relation

$$A_p = aT_\|^b \tag{8}$$

where a and b are constants. When all 373 events are included, a fit to the data gives a = 1.03 and b = −0.14 with R = −0.28. A fit to the data for each MLT sector results in different values of a, b, and R, as shown in Table 2a. Table 2b summarizes the radial variation of the $A_p - T_\|$ relation in equation (8).

[47] We again see that the coefficients a and b in equation (8) vary with local time and L value. This is what is expected from the argument presented by *Gary et al.* [1994b], as described in section 5.1.

6. Conclusions

[48] In summary, in this study data from 59 days in 1986, obtained by the SCATHA satellite, have been analyzed to identify the electromagnetic ion cyclotron waves in the Earth's magnetosphere and to study the electromagnetic proton cyclotron instability as a generation mechanism for EMIC waves in the Earth's magnetosphere. Following the procedures outlined in sections 2.2 and 3, we selected 373 two-minute interval events for analysis that are from proton plasmas not influenced by heavier ions. These events occurred in all local time sectors, with L values from 5.6 to 8.1 and magnetic latitudes between −13.7° and 15.6°.

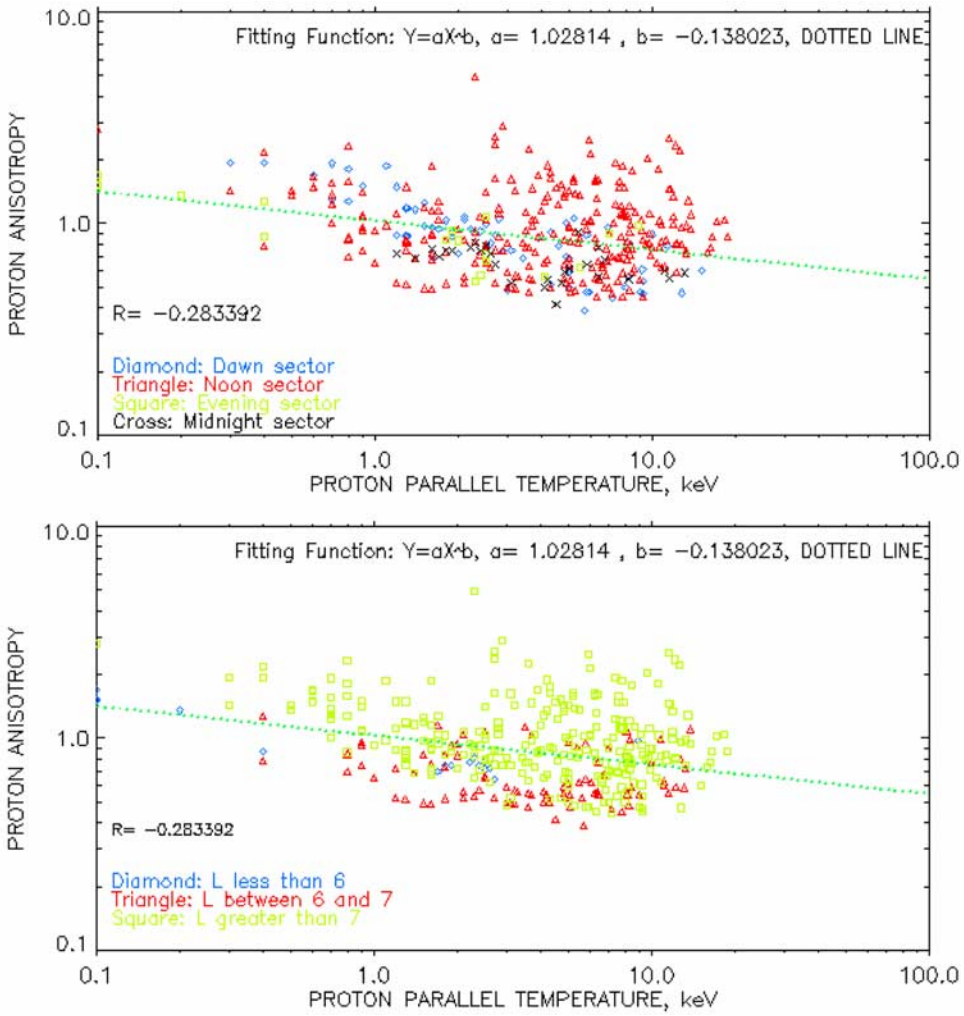

Figure 3. The upper panel shows a scatterplot of proton anisotropy versus proton parallel temperature with the data binned by MLT values and color-coded; the dotted line is the fitting curve for all data. The lower panel shows the same scatterplot as the upper panel, but the data are binned by L values.

For each event, in the FAC system, the values of P_{tran} are significantly greater that those of corresponding P_{para}, consistent with the expectation of field-aligned propagating EMIC waves.

[49] From this study the following conclusions can be drawn:

[50] 1) There are several findings that are consistent with those of previous studies and/or with theoretical expectations. They include (a) the inverse correlation between proton temperature anisotropy and hot proton parallel beta and that the observed A_p are near the electromagnetic proton cyclotron instability thresholds, and (b) that the observed waves actually get energy from energetic and anisotropic proton populations.

[51] 2) Owing to the large number of events and the complete set of data accompanying each, we are able to study predicted theoretical relationships as a function of MLT and L. Analysis of the results yields a new empirical expression for A_p as a function of the hot proton parallel beta, $\beta_{\|h}$, and the maximum value of the wave temporal growth rate. We found that the relation $A_p = S_h(\gamma_m/\Omega_P)^M \beta_{\|h}^{\alpha_h}$ shows a strong correlation with the data when all events are considered together and when events are grouped in different local time sectors and L ranges. A power law relation between A_p and $T_{\|}$, given by equation $A_p = aT_{\|}^b$, also shows a strong correlation with the data for all events and for those in different MLT sectors and L ranges. The finding that the coefficients depend on macroscopic factors such as local time and L value reflects the degree of strength

Table 2a. Summary of the Relationship Between A_p and $T_{\|}$ Through the Coefficients a and b of the Relation $A_p = aT_{\|}^b$ and the Correlation Coefficients R for Different MLT Sectors

MLT	a	b	R	No. of Events
03 < MLT < 09 (Dawn sector)	1.28	−0.39	−0.80	67
09 < MLT < 15 (Noon sector)	0.95	−0.06	−0.13	256
15 < MLT < 21 (Evening sector)	0.91	−0.22	−0.82	22
21 < MLT < 03 (Midnight sector)	0.82	−0.16	−0.47	28
All	1.03	−0.14	−0.28	373

Table 2b. Summary of the Relationship Between A_p and $T_{\|}$ Through the Coefficients a and b of the Relation $A_p = aT_{\|}^b$ and the Correlation Coefficients R for Different L Ranges

L value	a	b	R	No. of Events
L < 6	0.90	−0.23	−0.89	20
6 < L < 7	0.68	−0.09	−0.18	90
L > 7	1.16	−0.16	−0.31	263
All	1.03	−0.14	−0.28	373

of external forces driving the energetic proton temperature anisotropy.

[52] **Acknowledgments.** This study is supported in part by NASA, contract NAS5-96020.

[53] Zuyin Pu thanks the reviewers for their assistance in evaluating this paper.

References

Anderson, B. J., and S. A. Fuselier (1993), Magnetic pulsations from 0.2 to 4 Hz and associated plasma properties in the Earth's subsolar magnetosheath and plasma depletion layer, *J. Geophys. Res.*, *98*, 1461.

Anderson, B. J., and D. C. Hamilton (1993), Electromagnetic Ion Cyclotron Waves Stimulated by Modest Magnetospheric Compressions, *J. Geophys. Res.*, *98*, 11,369–11,382.

Anderson, B. J., K. Takahashi, R. E. Erlandson, and L. J. Zanetti (1990), Pc1 pulsations observed by AMPTE/CCE in the Earth's outer magnetosphere, *Geophys. Res. Lett.*, *17*, 1853.

Anderson, B. J., R. E. Erlandson, and L. J. Zanetti (1992a), A statistical study of Pc1-2 magnetic pulsations in the equatorial magnetosphere: 1. Equatorial occurrence distribution, *J. Geophys. Res.*, *97*, 3075.

Anderson, B. J., R. E. Erlandson, and L. J. Zanetti (1992b), A statistical study of Pc1-2 magnetic pulsations in the equatorial magnetosphere: 2. Wave properties, *J. Geophys. Res.*, *97*, 3089.

Anderson, B. J., S. A. Fuselier, S. P. Gary, and R. E. Denton (1994), Magnetic spectral signatures in the Earth's subsolar magnetosheath and plasma depletion layer, *J. Geophys. Res.*, *99*, 5877.

Anderson, B. J., R. E. Denton, G. Ho, D. C. Hamilton, S. A. Fuselier, and R. J. Strangeway (1996), Observational test of local proton cyclotron instability in the Earth's magnetosphere, *J. Geophys. Res.*, *101*, 21,527–21,543.

Bossen, M., R. L. McPherron, and C. T. Russell (1976), A statistical study of Pc1 magnetic pulsations at synchronous orbit, *J. Geophys. Res.*, *81*, 6083.

Chappell, C. R. (1974), Detached plasma regions in the magnetosphere, *J. Geophys. Res.*, *79*, 1861.

Cornwall, J. M. (1965), Cyclotron instabilities and electromagnetic emissions in the ultra-low frequency and very-low frequency ranges, *J. Geophys. Res.*, *70*, 61.

Denton, R. E., J. Goldstein, and J. D. Menietti (2002), Field line dependence of magnetospheric electron density, *Geophys. Res. Lett.*, *29*(24), 2205, doi:10.1029/2002GL015963.

Fennell, J. F., G. M. Boyd, M. T. Redding, and M. C. McNab (1997), Data Recovery from SCATHA satellite, Prepared for European Space Research and Technology Centre, Noordwijk, The Netherlands, Contract No. 11006/94/NL/CC and National Aeronautics and Space Administration, Washington, D. C. 20546, Grant No. NAGW-4141, Space and Environment Technology Center, the Aerospace Corporation.

Fraser, B. J. (1985), Observations of ion cyclotron waves near synchronous orbit and on the ground, *Space Sci. Rev.*, *42*, 357.

Fraser, B. J., and R. L. McPherron (1982), Pc1-2 magnetic pulsation spectra and heavy ion effects at synchronous orbit: ATS-6 results, *J. Geophys. Res.*, *87*, 4560.

Fraser, B. J., and T. S. Nguyen (2001), Is the plasmapause a preferred source region of electromagnetic cyclotron waves in the magnetosphere, *J. Atmos. Sol. Ter. Phys.*, *63*, 1225.

Fraser, B. J., W. J. Kemp, and D. J. Webster (1989), Ground-Satellite Study of a Pc 1 Ion Cyclotron Wave Event, *J. Geophys. Res.*, *94*, 11,855–11,863.

Fraser, B. J., J. C. Samson, Y. D. Hu, R. L. McPherron, and C. T. Russell (1992), Electromagnetic ion cyclotron waves observed near the oxygen cyclotron frequency by ISEE 1 and 2, *J. Geophys. Res.*, *97*, 3063.

Fraser, B. J., H. J. Singer, M. L. Adrian, and D. L. Gallagher (2005), The Relationship between Plasma Density Structure and EMIC Waves at Geosynchronous Orbit, in *Inner Magnetosphere Interactions: New Perspectives from Imaging Geophys. Monogr. Ser. 159*, edited by J. L. Burch, M. Schulz, and H. E. Spence, AGU.

Gary, S. P. (1993), *Theory of space plasma microinstabilities, Cambridge Atmospheric and Space Science Series*, p. 128, Cambridge Univ. Press.

Gary, S. P., and M. A. Lee (1994), The ion cyclotron instability and the inverse beta correlation between proton anisotropy and proton beta, *J. Geophys. Res.*, *99*, 11,297.

Gary, S. P., M. D. Montgomery, D. W. Feldman, and D. W. Forslund (1976), Proton temperature anisotropy instability in the solar wind, *J. Geophys. Res.*, *81*, 1241.

Gary, S. P., M. E. McKean, D. Winske, B. J. Anderson, R. E. Denton, and S. A. Fuselier (1994a), Proton cyclotron anisotropy and the anisotropy/beta inverse correlation, *J. Geophys. Res.*, *99*, 5903.

Gary, S. P., M. B. Moldwin, M. F. Thomsen, D. Winske, and D. J. McComas (1994b), Hot proton anisotropies and cool proton temperatures in the magnetosphere, *J. Geophys. Res.*, *99*, 23,603.

Gomberoff, L., and S. Cuperman (1982), Combined Effect of Cold H^+ and He^+ Ions on the Proton Cyclotron Electromagnetic Instability, *J. Geophys. Res.*, *87*, 95–100.

Gomberoff, L., and R. Neira (1983), Convective growth rate of ion cyclotron waves in a H^+-He^+ and H^+-He^+-O^+ plasma, *J. Geophys. Res.*, *88*, 2170.

Ishida, J., S. Kokubun, and R. L. McPherron (1987), Substorm effects on spectral structures of Pc1 waves at synchronous orbit, *J. Geophys. Res.*, *92*, 143.

Jordanova, V. K., C. J. Farrugia, R. M. Thorne, G. V. Khazanov, G. D. Reeves, and M. F. Thomsen (2001), Model of the ring current proton precipitation by electromagnetic ion cyclotron waves during the May 14–16, 1997, storm, *J. Geophys. Res.*, *106*, 7.

Kallenrode, May-Britt (2001), *Space physics: an introduction to plasmas and particles in the heliosphere and magnetospheres*, 2nd ed., Springer.

Kaye, S. M., and M. G. Kivelson (1979), Observations of Pc1-2 waves in the outer magnetosphere, *J. Geophys. Res.*, *84*, 4267.

Kennel, C. F., and H. E. Petschek (1966), Limit on stably trapped particle fluxes, *J. Geophys. Res.*, *71*, 1–28.

Kozyra, J. U., T. E. Cravens, A. F. Nagy, E. G. Fontheim, and R. S. B. Ong (1984), Effects of energetic heavy ions on electromagnetic ion cyclotron wave generation in the plasmapause region, *J. Geophys. Res.*, *99*, 2217–2233.

Kozyra, J. U., V. K. Jordanova, R. B. Horne, and R. M. Thorne (1997), Modeling of the contribution of Electromagnetic Ion Cyclotron (EMIC) waves to stormtime ring current erosion, in magnetic storms, *Geophys. Monogr.*, *98*, 187–202.

Mauk, B. H., and R. L. McPherron (1980), An experimental test of the electromagnetic ion cyclotron instability within the Earth's magnetosphere, *Phys. Fluid*, *23*, 2111.

Perraut, S., R. Gendrin, A. Roux, and C. de Villedary (1984), Ion Cyclotron Waves: Direct Comparison between Ground-Based Measurements and Observations in the Source Region, *J. Geophys. Res.*, *89*, 195.

Rauch, J. L., and A. Roux (1982), Ray tracing of ULF waves in a multicomponent magnetospheric plasma: Consequences for the generation of ion cyclotron waves, *J. Geophys. Res.*, *87*, 8191.

Roux, A., S. Perraut, J. L. Rauch, C. de Villedary, G. Kremser, A. Korth, and D. T. Young (1982), Wave-particle interactions near Ω^+_{He} observed on GEOS 1 and 2, 2. Generation of ion cyclotron waves and heating of He^+ ions, *J. Geophys. Res.*, *82*, 8174.

Samsonov, A. A., M. I. Pudovkin, S. P. Gary, and D. Hubert (2001), Anisotropic MHD model of the dayside magnetosheath downstream of the oblique bow shock, *J. Geophys. Res.*, *106*, 21,689–21,699.

Sheeley, B. W., M. B. Moldwin, and H. K. Rassoul (2001), An empirical plasmasphere and trough density model: CRRES observations, *J. Geophys. Res.*, *106*(A11), 25,631.

Spence, H. E., A. M. Jorgensen, W. J. Hughes, J. F. Fennell, and J. L. Roeder (1997), Towards inner magnetosphere particle and field models, *Adv. Space Res.*, *20*(3), 427–430, Published by Elsevier Ltd, Pergamon.

Stevens, R. J., and A. L. Vampola (1978), Description of the space test program P78-2 spacecraft and payloads, report *SAMSO TR-78-24*, The Aerospace Corporation.

Swanson, D. G. (2003), *Plasma waves (Second edition), Institute of Physics, Series in Plasma Physics*, Taylor and Francis Publisher.

Thorne, R. M., and R. B. Horne (1994), Energy transfer between energetic ring current H^+ and O^+ by electromagnetic ion cyclotron waves, *J. Geophys. Res.*, *90*, 17,275–17,282.

Thorne, R. M., and R. B. Horne (1997), Modulation of electromagnetic ion cyclotron instability due to interacton with ring current O+ during magnetic storms, *J. Geophys. Res.*, *102*, 14,155–14,163.

Xue, S., D. M. Thorne, and D. Summers (1996), Parametric study of electromagnetic ion cyclotron instability in the Earth's magnetosphere, *J. Geophys. Res.*, *101*, 15,467–15,474.

Young, D. T., S. Perraut, A. Roux, C. de Villedary, R. Gendrin, A. Korth, G. Kremser, and D. Jones (1981), Wave-particle interactions near Ω^+_{He}

observed on GEOS 1 and 2, 1. Propagation of ion cyclotron waves in He^+-rich plasma, *J. Geophys. Res.*, *86*, 6755.

J. F. Fennell, Space Science Laboratory, the Aerospace Corporation, El Segundo, CA 90245, USA. (joseph.f.fennell@aero.org)

S. T. Nguyen, The Pre-University School of Hochiminh City, 91 Nguyen chi Thanh Street, District 5, Hochiminh City, Vietnam. (nguyenthanhson56@hotmail.com)

J. D. Perez, Allison Laboratory, Auburn University, Auburn, AL 36849, USA. (perez@physics.auburn.edu)